Fernando Ramírez P., Fernando; Soldani, Xavier; Loya, José; Miguélez, Henar (2017). A new approach for time-space wear modeling applied to machining tool wear, *Wear*, v. 390-391, pp.: 125-134.

DOI: https://doi.org/10.1016/j.wear.2017.07.015

A new approach for time-space wear modeling applied to machining tool wear

Fernando Ramírez P.[a,b,*], Xavier Soldani[b], José Loya[c], Henar Miguélez[b]

[a] Faculty of Engineering and Applied Science, Universidad Técnica del Norte, Avda. 17 de Julio 5-21, 100105 Ibarra, Ecuador
[b] Department of Mechanical Engineering, Universidad Carlos III de Madrid, Avda. de la Universidad 30, 28911 Leganés, Madrid, Spain
[c] Department of Continuum Mechanics and Structural Analysis, Universidad Carlos III de Madrid, Avda. de la Universidad 30, 28911 Leganés, Madrid, Spain

ARTICLE INFO

Keywords:
Wear modeling
Metal cutting
Crater wear
FEM
AISI 1018
Dimensional analysis

ABSTRACT

A general methodology is proposed and demonstrated for modeling the progression of crater wear on cutting tools used for steel machining. Dimensional analysis and Finite Element Analysis of metal cutting are the foundations of this new approach. The dimensional analysis resulted in a differential equation which describes wear rate as a function of dimensionless variables. Numerical models of cutting allow one to estimate local variables associated with wear at tool-chip contact. Orthogonal cutting simulations were carried out with commercial code DEFORM - 2D Ver 11.0. AISI 1018 steel was used as the workpiece material for an uncoated carbide cutting tool. Prediction of wear evolution and crater profiles on the tool's rake face were in good agreement with experimental data.

1. Introduction

Cutting tool wear has an important impact in machining economics. Prevention of tool wear and replacement of worn cutting tools represent about 18–24% of machining costs [1,2]. From a global point of view, the effect of tool wear could be summarized by analyze energy consumption. Machining processes consume about 30–50% of the energy demanded by industry. Industrialized countries destine about 31–45% of their total energy for industrial processes. The information above allows to see that cutting tool wear has a significative economical and environmental impact. Machining processes are still the fundamental manufacturing techniques and it is expected to remain so for the next few decades. This fact explains the intense research activity about the cutting tool wear processes [3–8].

Flank wear and crater wear are the most common parameters for tool life estimation in metal cutting [9,10] (see Fig. 1 (a)). When a cutting tool reaches the end of its useful life, it can no longer produce machined parts with the desired dimensions and surface quality. Special norms regarding tool wear criteria have been established to define cutting tool life. For low and medium cutting speeds, tool life is a function of flank wear land V_B. On the other hand, for high cutting speeds tool life is a function of maximum crater depth K_T and feed t_1 [11,12].

In order to estimate tool life, Taylor proposed an empirical equation which was based on referential tool life and cutting speed [13]. Since then, several tool life equations and tool wear models have been proposed (crater and flank). The basic wear mechanisms observed in carbide tools for metal cutting are: Adhesion, Abrasion and Diffusion thermally activated [14–16]. Adhesion mechanism causes loss of material due to the combination of high contact pressure and relative movement in tool-chip interface. High pressure generates welded junctions at tool-chip contact and relative movement produces tearing at welded junctions with loss of material at tool rake face [17]. Abrasion mechanism generates loss of material by the action of hard asperities or particles at tool-chip interface [18]. Diffusion is characterized by movement of atoms from tool to chip and vice-versa. The relative movement at tool-chip interface carries away tool material forming a crater [14,19].

For wear modeling, different combinations of wear mechanisms have been taken into account: diffusive [14,20,21], abrasive and adhesive [22,23], abrasive and diffusive [24], adhesive and diffusive [25], abrasive and dissolution [26], and other wear models which are functions of machining parameters as cutting speed [27,28].

All of the wear mechanisms on tool-chip interface are related to different local variables at contact interface. As a result of this, in the wear models developed the wear rate depends, among other things, on local variables at contact interface as normal stress σ_n, sliding velocity V_s, temperature T_{int} and material constants [29].

For tool wear prediction using the models above-mentioned it is common to employ constant values of local variables (maximum or

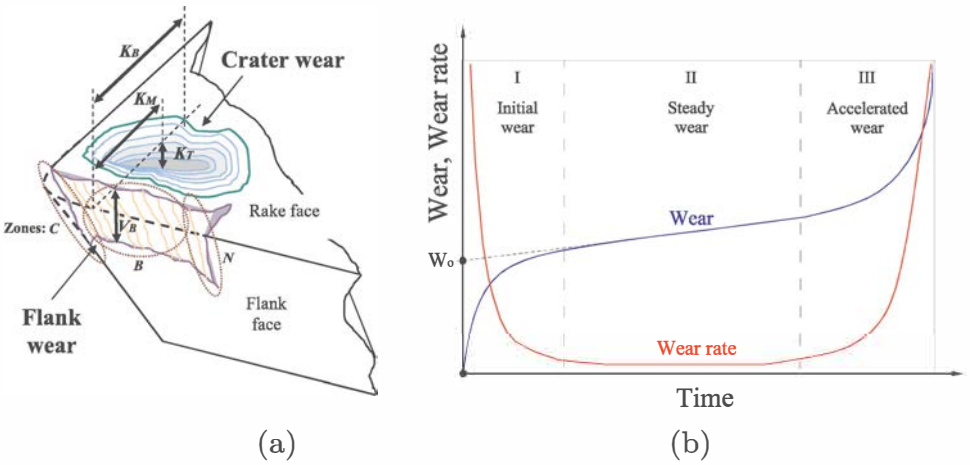

Fig. 1. Cutting tool wear: (a) Crater wear (K_B, K_M y K_T), and Flank wear (V_B); (b) characteristic wear evolution: I: Initial wear; II: Steady state, III: Accelerated wear.

average values). This is because it is not possible to accurately predict the time-space behaviour of local variables through the wear process at tool-chip contact interface [30–32]. As a consequence of this, wear rate defined as a function of local variables stays constant throughout the machining process for traditional wear modeling.

To consider wear rate as constant in wear process modeling is not in accordance with experimental evidence. Fig. 1(b) shows typical wear evolution with time. It is possible to see three well-defined zones: I: Initial wear, II: Steady wear and III: Accelerated or Severe wear. In the first zone the wear rate decreases rapidly until reaching a steady state. In the second zone the wear rate remains approximately constant. This period of time is known as the useful tool life. In the third zone the wear rate suffers a strong increment until reaching catastrophic tool failure [33].

Traditional wear models are focused on predicting tool wear in Zone II. If wear rate is considered as a constant in time, the only way to accurately predict the wear behaviour in that zone is by having an initial wear W_o which is different from zero (Fig. 1, (b)). Experimentally, it has been observed that a sudden flank wear occurred in the few cutting instants of machining processes [21]. However, due to the thermo-mechanical nature of wear, after this sudden flank at the beginning of the process, wear evolution was progressive and non-immediately linear. All of the above-mentioned suggests that it is important to take Zone I: Initial wear into account in order to accurately model wear evolution. In other words: for wear modeling it is important to consider wear rate as non-constant in time.

The new approach proposed in this paper has been focused on crater wear modeling. The modeling methodology followed begins by defining wear phenomena into a discretized worn surface. The second step consists of the development of a wear differential equation by using dimensional analysis. This general equation describes wear rate as a function of non-dimensional variables. The third step is to model orthogonal cutting by FEM. This stage allows one to obtain the local variables' distribution along the worn surface for model calibration. The results reached were compared to experimental evidence with strong agreement.

2. Material and methods

For calibration and validation, experimental results from specialized literature have been used [34]. Wear tests have been carried out by reproducing orthogonal cutting conditions. Workpiece material was AISI 1018 steel. Cutting tools used were plain uncoated carbide inserts. Fig. 2 shows an schema about orthogonal cutting. For all of the tests rake angle $\alpha = 0°$ and clearance angle $\beta = 6°$. Cutting speed V_c covers $100 - 400$ m/min range. Feed t_1 covers $0.1 - 0.3$ mm range. Cutting edge radius was $R = 20$ μm.

3. Methodology for wear modeling

3.1. Discretization of worn surface

Wear process at tool-chip interface is due to a combination of different local variables acting on contact interface. The wear rate is non constant along tool-chip contact. The topography generated by lost of material is complex and non-uniform. In order to establish a relationship between the different combinations of local variables and the material lost, the worn surface has been divided into smaller worn subzones (See Fig. 3).

In this work an orthogonal cutting approach has been used for metal cutting simulations. From this point of view the discretization of worn surface is changed into the discretization of a strength line (p axis in Fig. 3).

3.2. Development of a characteristic wear equation

For the development of a characteristic equation to describe wear rate has been proposed the existence of a function f such as:

$$f(\rho, C_p, R, E, V_s, \sigma_n, T_{int}, K_T, t) = 0 \quad (1)$$

where ρ and C_p are the density and specific heat of tool material respectively. R is the gas constant and E is the activation energy relative to 1 mol of substance. T_{int} is the interface temperature, σ_n is the normal pressure, V_s is the sliding velocity at the tool-chip contact. K_T is the depth of crater and t is the time. Variables T_{int}, σ_n and V_s are called wear variables and their value is constant in time for each cutting conditions. This values are taken from steady-state stage of orthogonal cutting simulations.

The Vaschy-Buckingham theorem applied to Eq. (1) affirms that there is a dimensionless function ϕ_1 equivalent to f such as:

$$\phi_1(\pi_i) = 0; \quad i = 1, 2, \ldots, 5 \quad (2)$$

where π_i are dimensionless variables (dimension $[\pi_i] = 1$), constructed as different combinations of the parameters: ρ, C_p, R, E, V_s, σ_n, T_{int}, K_T, t raised to $\lambda_{i,j}$-th power as shows Eq. (3).

$$[\pi_i] = [\rho]^{\lambda_{i,1}}[C_p]^{\lambda_{i,2}}[R]^{\lambda_{i,3}}[E]^{\lambda_{i,4}}[V_s]^{\lambda_{i,5}}[\sigma_n]^{\lambda_{i,6}}[T_{int}]^{\lambda_{i,7}}[K_T]^{\lambda_{i,8}}[t]^{\lambda_{i,9}} \quad (3)$$

Where $\lambda_{i,j}$ are constants, i corresponds to the π_i dimensionless variables and j corresponds to each one of the physical parameters from Eq. (1). Taking account that $[\pi_i] = 1$ plus dimensional information shown in Table 1 it is possible to establish the System of Eq. (4).

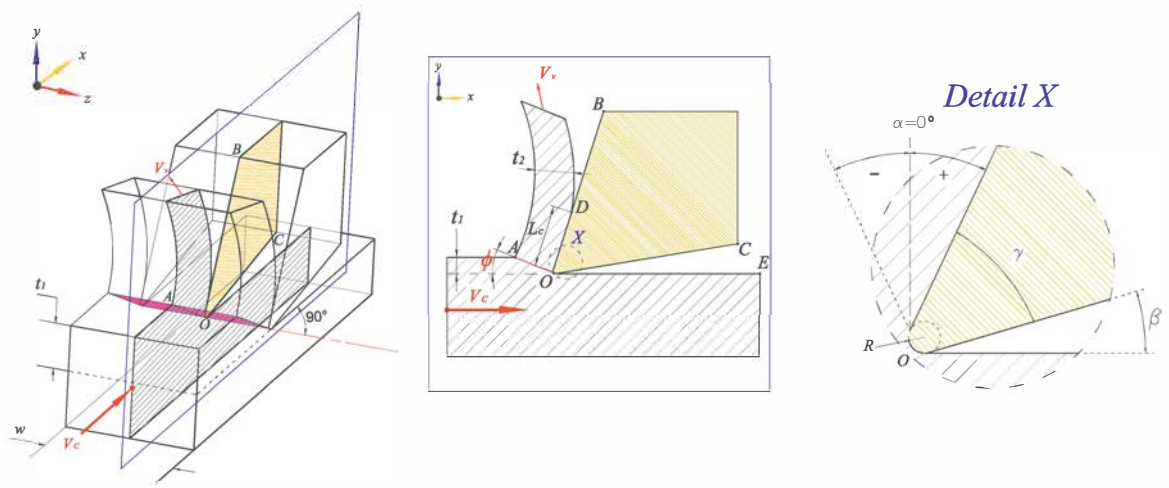

Fig. 2. Orthogonal cutting: (a) plane strain deformation hypothesis; (b) plane of metal cutting; (c) cutting geometry.

$$\begin{bmatrix} -3 & 2 & 2 & 2 & 1 & -1 & 0 & 1 & 0 \\ 1 & 0 & 1 & 1 & 0 & 1 & 0 & 0 & 0 \\ 0 & -2 & -2 & -2 & -1 & -2 & 0 & 0 & 1 \\ 0 & -1 & -1 & 0 & 0 & 0 & 1 & 0 & 0 \end{bmatrix} \begin{bmatrix} \lambda_{i,1} \\ \lambda_{i,2} \\ \vdots \\ \lambda_{i,9} \end{bmatrix} = \begin{bmatrix} 0 \\ 0 \\ 0 \\ 0 \end{bmatrix} \tag{4}$$

The solution of System (4) gives the Eq. (5) which rules the set of constants $\{\lambda_{i,j} | i = 1-5;\ j = 1-9\}$.

$$\left.\begin{aligned} \lambda_{i,1} &= \tfrac{1}{3}\lambda_{i,8} - \lambda_{i,6} + \tfrac{1}{3}\lambda_{i,9} \\ \lambda_{i,2} &= \tfrac{1}{3}\lambda_{i,8} - \lambda_{i,6} - \tfrac{1}{2}\lambda_{i,5} + \tfrac{5}{6}\lambda_{i,9} \\ \lambda_{i,3} &= \tfrac{1}{2}\lambda_{i,5} + \lambda_{i,6} + \lambda_{i,7} - \tfrac{1}{3}\lambda_{i,8} - \tfrac{5}{6}\lambda_{i,9} \\ \lambda_{i,4} &= \tfrac{1}{2}\lambda_{i,9} - \lambda_{i,6} - \lambda_{i,7} - \tfrac{1}{2}\lambda_{i,5} \\ \lambda_{i,5},\ \lambda_{i,6},\ \lambda_{i,7},\ \lambda_{i,8},\ \lambda_{i,9} &\ \ independent \end{aligned}\right\} \tag{5}$$

Thus, wear modeling depends on dimensionless variables π_i. Each one of π_i is variable on time and space, and its internal structure reflects this variability by three sub-products: Material constants: $\Pi_{\mathbf{C}_i} = (\rho)^{\lambda_{i,1}}(C_p)^{\lambda_{i,2}}(R)^{\lambda_{i,3}}(E)^{\lambda_{i,4}}$, Wear variables: $\Pi_{\mathbf{W}_i} = (V_s)^{\lambda_{i,5}}(\sigma_n)^{\lambda_{i,6}}(T_{int})^{\lambda_{i,7}}$, which is variable on space, and Input-Output variables in the model: $\Pi_{\mathbf{O}_i} = (K_T)^{\lambda_{i,8}}(t)^{\lambda_{i,9}}$, variable on time. This allows to rewrite Eq. (1) as Eq. (6).

$$\pi_i = \Pi_{\mathbf{C}_i} \cdot \Pi_{\mathbf{W}_i} \cdot \Pi_{\mathbf{O}_i};\ \ i = 1, 2, \ldots, 5 \tag{6}$$

Based on Eq. (2) the variable π_1 can be represented as a new dimensionless function $\phi_2(\pi_2, \ldots, \pi_5)$. If π_1 is written by using Eq. (6) it is possible to obtain $K_T(t)$ as shows Eq. (7).

$$K_T(t) = \left[\frac{1}{\Pi_{\mathbf{C}_1} \cdot \Pi_{\mathbf{W}_1} \cdot (t)^{\lambda_{1,9}}} \cdot \phi_2(\pi_2, \pi_3, \pi_4, \pi_5)\right]^{1/\lambda_{1,8}} \tag{7}$$

Eq. (7) allows to obtain a general expression for crater wear rate by time derivative. The primary result of this process is showed in Eq. (8).

$$\frac{\partial K_T}{\partial t} = \frac{1}{\lambda_{1,8}} \cdot \frac{K_T}{\pi_1} \cdot \left\{ \frac{\partial \phi_2}{\partial t} - \phi_2 \cdot \frac{\partial}{\partial t}\left[\ln\left(\Pi_{\mathbf{C}_1} \cdot \Pi_{\mathbf{W}_1} \cdot t^{\lambda_{1,9}}\right)\right] \right\} \tag{8}$$

The time derivative of dimensionless function $\phi_2(\pi_2, \ldots, \pi_5)$ is indicated in Eq. (9). The additive nature of this mathematical expression shows that $\phi_2(\pi_2, \ldots, \pi_5)$ summarizes the effect of distinct wear mechanisms acting on worn surface.

$$\frac{\partial \phi_2}{\partial t} = \sum_{i=2}^{5} \frac{\partial \phi_2}{\partial \pi_i} \frac{\partial \pi_i}{\partial t} \tag{9}$$

To continue with the wear model development there are some mathematical requirements: Time variability of π_1 depends only on K_T, it means that $\lambda_{1,8} \neq 0$, $\lambda_{1,9} = 0$ and $\lambda_{i,8} = 0$, $i = 2, \ldots, 5$. At least one of the π_i, $i = 2, \ldots, 5$ must depend on t, it means that at least one of $\lambda_{i,9} \neq 0$ for $i = 2, \ldots, 5$. All of the requirements exposed above lead to the general Eq. (10).

$$\frac{\partial K_T}{\partial t} = \frac{K_T}{\lambda_{1,8} \cdot \pi_1 \cdot t} \sum_{i=2}^{5} \frac{\partial \phi_2}{\partial \pi_i} \cdot \pi_i \cdot \lambda_{i,9} \tag{10}$$

Based on experimental observations, it is possible to describe Wear rate behaviour in Zones I and II (See Fig. 1 (b)), by using a potential function on time. For that reason function ϕ_2 has been defined as is indicated in Eq. (11).

$$\phi_2 = \frac{A}{n+1} \cdot \pi_2^{n+1} + \phi_3(\pi_3, \pi_4, \pi_5) \tag{11}$$

Where A, n are constants of model. Function ϕ_3 is a new dimensionless function depending on π_3, π_4, π_5. For wear modeling in this

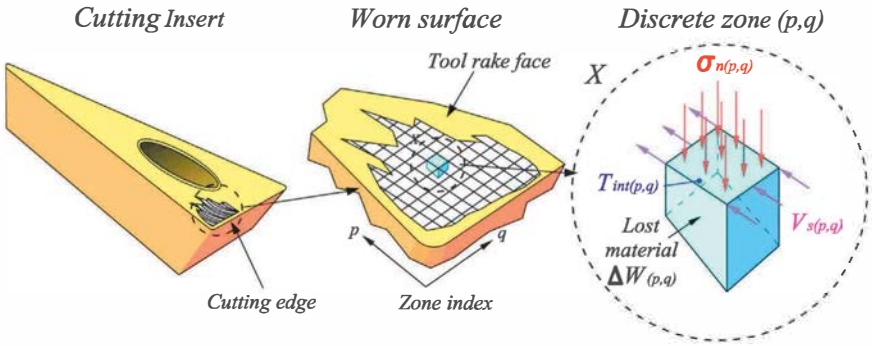

Fig. 3. Discretization of worn surface for spatial wear analysis.

Table 1
Dimensional equivalence of the variables and constants involved into Eq. (1).

$[\rho]$	$[C_p]$	$[R]$	$[E]$	$[V_s]$	$[\sigma_n]$	$[T_{int}]$	$[K_T]$	$[t]$
$L^{-3}M$	$L^2T^{-2}\Theta^{-1}$	$L^2MT^{-2}\Theta^{-1}N^{-1}$	$L^2MT^{-2}N^{-1}$	LT^{-1}	$L^{-1}MT^{-2}$	Θ	L	T

work it has been considered that variables π_3, π_4, π_5 are not depending on time t ($\lambda_{3,9} = \lambda_{4,9} = \lambda_{5,9} = 0$). This consideration means that the effect of all the wear mechanisms acting on tool-chip contact is going to be summarized by an only one dimensionless variable π_2. Variable π_1 change linearly whit K_T ($\lambda_{1,8} = 1$) and wear variables T_{int}, σ_n and V_s, have the same influence on π_1 and π_2 ($\Pi_{W_1} = \Pi_{W_2}$). By replacing Eq. (11) in (10) is obtained the crater wear model (Eq. (12)).

$$\frac{\partial K_T}{\partial t} = \frac{\Pi_{C_2}}{\Pi_{C_1}} \cdot \lambda_{2,9} \cdot t^{\lambda_{2,9}-1} \cdot A\pi_2^n \tag{12}$$

Thus, it has been applied a new methodology for wear modeling in order to develop a general wear equation (Eq. (10)). Based on this general equation it has been developed a specific crater wear model (Eq. (12)), by using an only one dimensionless variable π_2, which summarizes the effect of all the wear mechanisms acting on tool-chip interface. In order to calibrate the developed wear model by using wear variables distributions is necessary to carry out numerical simulations of metal cutting.

4. Numerical simulation of orthogonal cutting

Crater wear depends on wear variables distributions on tool-chip contact (Eq. (1)). These distributions are very hard to be observed experimentally. For that reason, they have been obtained from numerical simulations of orthogonal cutting. All of the numerical models in this work have been developed by using commercial code DEFORM™- 2D/3D Ver 11.0. This FEA code has been developed by *Scientific Forming Technologies Corporation* (SFTC) whit updated Lagrangian formulation and automatic remeshing. It is focused to model metal forming, heat treatment and machining processes.

4.1. Material model

Chip morphology, temperatures and cutting forces in orthogonal cutting simulations are influenced principally by material model, friction model and temperatures at tool-chip contact [35]. In this work carbide cutting tool has been considered as a rigid body. The workpiece material follows a thermo-viscoplastic behaviour described by the Johnson–Cook's law (Eq. (13)). In metal cutting FEM models, this material model is very used because it is able to describe accurately the material behaviour at high temperatures, high strains, and high strain-rates [36–40].

$$\sigma(\varepsilon, \dot{\varepsilon}, T) = (\sigma_0 + B\varepsilon^n)\left(1 + C\, ln\frac{\dot{\varepsilon}}{\dot{\varepsilon}_0}\right)\left[1 - \left(\frac{T - T_r}{T_m - T_r}\right)^m\right] \tag{13}$$

Where σ is the material flow stress, ε is the plastic strain, $\dot{\varepsilon}$ is the strain rate, T is the temperature of the material. σ_0 is the yield stress, B is the hardening modulus and n is the strain-hardening exponent. C is the strain rate sensitivity and $\dot{\varepsilon_0}$ is the reference strain rate. T_m is the melting point of the material, T_r is the room temperature and m is the thermal-softening exponent or thermal sensitivity. The parameters used to represent the response of mild steel AISI 1018 in this work were calibrated by Sasso et al. [41] and have been used successfully in orthogonal cutting models [42]. The values of the parameters are given in Table 2.

Table 2
Set of parameters of the Johnson-Cook constitutive model for AISI 1018 [41].

	σ_0 [MPa]	B [MPa]	n	C	m	$\dot{\varepsilon}_0$ [s^{-1}]	T_r [K]	T_m [K]
AISI 1018	520	269	0.282	0.0476	0.53	1	293	1793

4.2. Friction model

In 1963 Zorev has proposed one of the most realistic friction models for machining simulations [43]. This approach divide the contact length in two regions: sliding and sticking, as is indicated in Fig. 4 (a).

Experimentally it has been observed that sliding region contribution to the shear and normal forces is relatively small compared with the contribution of the sticking region (Fig. 4(b)). This could be explained by the high contact pressures observed usually at tool-chip interface in metal cutting. Those contact pressures implies high cutting forces applied to very small contact areas giving as result high values of normal stress at tool-chip interface which cause the frictional stress over the most of contact region [46,47]. This observation has allowed to assume a frictional stress constant and proportional to the work material shear flow stress τ of the work material at the tool-chip interface as is indicated in Eq. (14) [48–50].

$$\tau_f = m_f\, \tau \tag{14}$$

Where τ_f is shear stress at tool-chip interface, τ is the shear flow stress of work material, m_f is the fraction of shear strength of work material. The *split cutting tool* technique used originally to establish the size of m_f has been complemented by measurement of temperature distribution over the rake face. Thus, the range of values $0.5 \leq m_f \leq 1$ has been tested with good thermal and mechanical results [48–54].

4.3. Thermal steady-state simulation

In order to reach steady-state temperatures at tool chip interface, in numerical simulations has been used the method proposed by Deshpande and Madhavan in [55]. This approach consists of reducing the value of specific heat C_p of cutting tool material to a virtual value C_{p-Num} to accelerate the temperatures stabilization.

Based on the modeling criteria exposed above, a set of numerical simulations of orthogonal cutting has been carried out. The C_p and m_f ranges covered were: $0.6 \leq m_f \leq 1$ and $0.002\, C_p \leq C_{p-Num} \leq C_p$. Numerical results obtained were compared to experimental data taken from specialized literature. The comparison variables were contact length, specific cutting pressure and tool temperature. The best global approximation of the numerical trends to the experimental data was reached by using $m_f = 0.6$ and $C_{p-Num} = 0.01\, C_p$ [56].

Geometrical parameters and border conditions used in numerical simulations are shown in Fig. 5 and reproduce experimental conditions from Section 2. Once numerical cutting simulations have been validated it is possible to get wear variables distribution onto tool rake face, showing good accordance with experimental evidence. Next step is to calibrate the wear model.

5. Calibration of developed crater wear model

The objective of calibration process is to set the constants A and n from Eq. (12). These constants are strongly related to some variable π_2 which has not been determined yet. This define calibration process as a

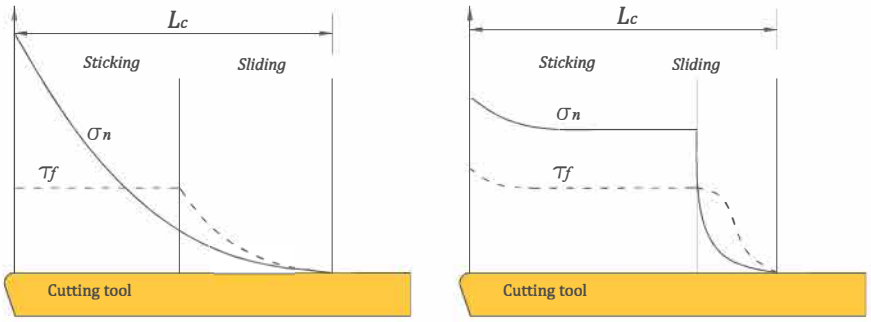

Fig. 4. Normal σ_n and frictional stress τ_f distribution along tool-chip interface: (a) Zorev's model of [43,44]; (b) schema based on experimental observations [45,46].

multi-objective optimization problem where π_2, A and n must be determined. Fig. 6 shows the algorithm of calibration followed.

The calibration process is founded on the experimental information that is shown in Table 3. Tests 1–4 were used for spatial calibration while test 5 was used for temporal calibration. Based on cutting conditions from experimental tests, numerical simulations of orthogonal cutting have been carried out. In this way the wear variables distributions T_{int}, σ_n, V_s on tool rake face have been determined.

Crater profiles for tests 1–4 (Table 3), have been interpolated by using polynomial functions as is shown in Fig. 7. This method is based on experimental observations which suggest, on the one hand, that crater profiles approximately reproduce temperatures shape on tool-chip contact and on the other hand, that experimental temperatures at tool-chip interface follow a polynomial law [57–59]. Fig. 8 shows numerical and interpolation results.

For tests 1–4 from Table 3 tool-chip contact has been divided into 20 discrete zones. A specific combination of wear variables (T_{int}, σ_n, V_s) which is represented by $A\pi_2^n$ (see Eq. (12)), is acting on each one of them and cause crater wear. The relationship between the specific wear rate on each discrete zone and the therm $A\pi_2^n$ has been established using an iterative least-squares regression process. The criterion for selecting π_2, A and n is the average correlation coefficient $\overline{R} \approx 1$ from all discrete zones.

Once π_2, A and n have been obtained the crater wear model is evaluated through a comparison with experimental results from Test 5. The final criterion for validating the wear model is the difference between $K_{T_{max}}$ predicted and experimental ($Err \approx 0$). The crater wear model calibrated is shown in Eqs. (15)–(16).

$$K_T(\xi, t) = \frac{A(\xi)}{n(\xi)+1} \cdot \frac{\rho^{k_1} C_p^{k_2} E^{k_3}}{R^{k_4}} \cdot \left(\frac{\sigma_n \, T_{int}^{\,7}}{\sqrt[4]{V_s^3}} \right)^{-n(\xi)} t^{\,5[n(\xi)+1]} \tag{15}$$

$$\xi = \frac{x}{L_c} \tag{16}$$

Where x is the position on tool rake face measured from cutting edge, L_c is the total tool-chip contact length, ξ is the dimensionless position taken from cutting edge. t is the time of machining. T_{int}, σ_n, V_s are respectively: interface temperature, normal pressure and sliding velocity (wear variables), at point where $K_T(\xi, t)$ is calculated. $A(\xi)$ and $n(\xi)$ values are indicated in Fig. 9 along tool-chip contact. ρ is the tool material density, C_p is the specific heat of tool material. R is the gas constant relative to 1 mol of substance, E is the activation energy relative to 1 mol of substance. k_1 to k_4 are functions of $n(\xi)$ and are described by Eq. (17).

$$\begin{aligned} k_1 &= \frac{4}{3}[1 + 2\,n(\xi)] \\ k_2 &= \frac{23}{24}[4 + 5\,n(\xi)] \\ k_3 &= \frac{1}{8}[20 + 81\,n(\xi)] \\ k_4 &= \frac{1}{24}[92 + 283\,n(\xi)] \end{aligned} \tag{17}$$

6. Results and discussion

6.1. About crater evolution

The evolution of the maximal crater depth for different cutting conditions are shown in Figs. 10, 12. Fig. 14(a) indicates the correlation between experimental data and wear model predictions for crater evolution. Experimental data has been taken from specialized literature [34]; meanwhile theoretical predictions have been made by using the developed crater wear model (Eq. (15)). Materials tested are AISI 1018 steel machined by orthogonal cutting with plain uncoated carbide cutting tool (rake angle $\alpha = 0°$, clearance angle $\beta = 6°$, cutting edge radius $R = 0.02$ [mm]). Cutting speed and feed covered ranges are: $V_c = 100 - 400$ [m/min] and $t_1 = 0.1 - 0.3$ [mm/rev] respectively. Numerical simulations of orthogonal cutting, necessaries for obtaining the inputs of crater wear model, have been carried out based on the experimental cutting conditions and parameters explained in Section 4.

The developed model (Eq. (15)), shows that crater wear phenomenon is governed mainly by temperature followed by sliding velocity and normal pressure. The comparison between experimental and

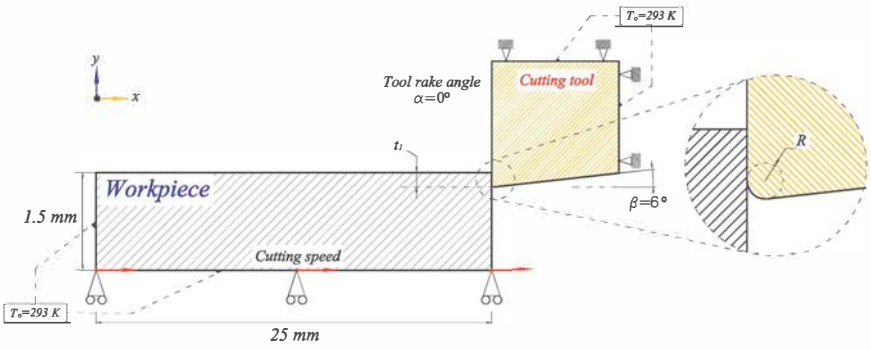

Fig. 5. Border conditions for orthogonal cutting simulations.

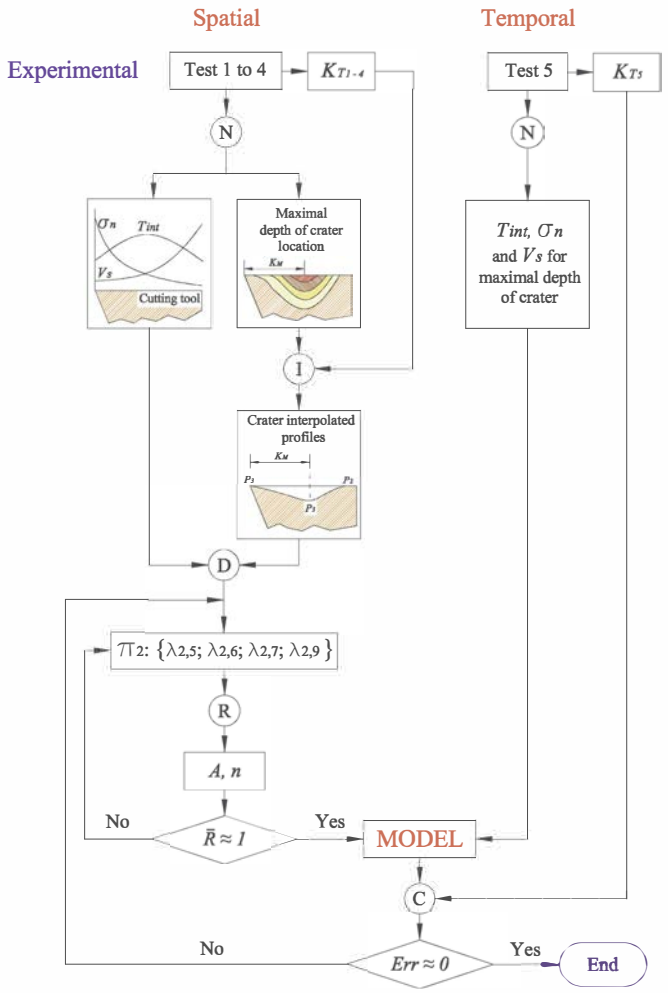

Fig. 6. Algorithm for calibration wear model: Ⓝ: numerical simulations of orthogonal cutting; Ⓘ: crater profiles interpolation; Ⓓ: discretization of tool-chip contact and wear variables distributions; ®: regression.

Table 3
Crater wear experimental results for calibration process. Materials: Tungsten Carbide (WC) and AISI 1018 steel. Feed: $t_1 = 0.1$ [mm]. Rake angle: $\alpha = 0°$, Clearance angle: $\beta = 6°$, Radius of cutting edge: $R = 0.02$ [mm] (See experimental detailed procedure in [34]).

Essay	Cutting speed V_c [m/min]	Time $[\Delta t]_{exp}$ [s]	K_{Texp} [mm]
1	100	333	0.021
2	200	118	0.043
3	300	45	0.061
4	400	7.8	0.057
5	100	1424.2	0.054

theoretical crater wear information has been made by two ways. The first one is to compare directly the experimental crater depth evolution with wear model predictions for different cutting conditions (Figs. 10 and 12). The second one consists into comparing K_T experimental and predicted value as fractions of maximal experimental depth of crater (Fig. 14(a)).

Through direct comparison it is possible to see that the results of crater evolution reached with wear model agrees well the trends observed experimentally. For cutting speeds lower than 200 [m/min] and feed equal to 0.1 [mm], theoretical predictions are closer to experimental evidence than at higher cutting speeds. For $V_c = 300 - 400$ [m/min] and feed 0.1 [mm] the numerical predictions are slightly lower than the experimental K_{Tmax} values. A similar behaviour can be noticed for $V_c = 200$ [m/min] and feed greater than 0.1 [mm] (Fig. 13).

The compared K_T fractions confirms the aforementioned observations. Fig. 14 (a) presents two well defined regions *A* and *B*. Region *A* shows high density of K_T dots and corresponds to cutting speeds lower than or equal to 200 [m/min] and feed equal to 0.1 [mm]. The trend followed by dots in this region (dashed line), presents a deviation equal to 9.88% of overestimation from K_T experimental. Region *B* shows low density of K_T dots and corresponds to cutting speeds greater than 200 [m/min] or feed equal to $0.2 - 0.3$ [mm]. The deviation observed in region *B* is an underestimation of 18.82% respect to K_T experimental. Taking account regions *A* and *B*, the general deviation of the model corresponds to an underestimation of 15.14% respect to experimental data.

The limit between regions *A* and *B* corresponds to cutting speed of 200 [m/min]. At this cutting speed the interface temperatures reached are around $1100 - 1200$ [K]. This change of trend indicated in Fig. 14(a) confirms the observations made by different researchers as a change of slope in crater evolution [25,60,61].

Changes in parameters as cutting speed or feed in machining processes modify significantly the values of wear variables at tool-chip contact. This could trigger different wear mechanisms on tool-chip interface [24,37,62]. Thus, the theoretical underestimation of K_{Tmax} by Eq. (15) could suggest the action of different wear mechanisms related to interface temperature increments for cutting speed greater than 200 [m/min] or feed greater than 0.1 [mm]. The proposed model can predict crater wear under the global effect of different wear mechanisms on tool-chip contact.

6.2. About crater profiles

Referential crater profiles have been obtained by following the interpolation process explained in Section 5. These results are compared with wear profiles generated by applying Eq. (15). Crater profiles comparison is shown in Figs. 11 and 13 for different cutting conditions. The profile trends obtained by using the developed model show good correspondence to those based on experimental results.

Also it has been analyzed the capability of the wear model to estimate the maximal crater depth location on tool rake face. The results are indicated in Fig. 14 (b). Maximal K_T location predicted by model is mainly concentrated in central region of contact length ($0.4 \leq \xi \leq 0.6$), where are also located the highest interface temperatures. This theoretical result has been demonstrated experimentally for different metal cutting researchers along XX century [9,63,64]. The trend followed by model prediction dots (dashed line), presents a deviation towards cutting edge of 3.47%. All of aforementioned observations show the good agreement between predicted K_T location and experimental observations.

6.3. About the influence of carbon content over crater wear

The developed wear model has been calibrated into a wide range of cutting conditions, for AISI 1018 steel and uncoated WC cutting tool. Due to the complexity of metal cutting process and the related tool wear evolution, any change on materials combination must be finally carefully observed. Thus, the applicability of crater wear model to different materials combination should be discussed. About this subject, Usui et al. proposed that in carbon steel machining the tool wear process are the same for similar work materials. It implies that wear mechanisms acting on tool-chip interface must be the same for similar carbon contents [25]. This hypothesis must be analyzed from the point of view of the effect of carbon content changes over wear variables T_{int}, σ_n, V_s.

The change in carbon content influences some material characteristics. For example, in carbon steel, as carbon is increased the hardness and strength also increase (Table 4). This increment has a negative impact over machining performance. Thus, it could be supposed that

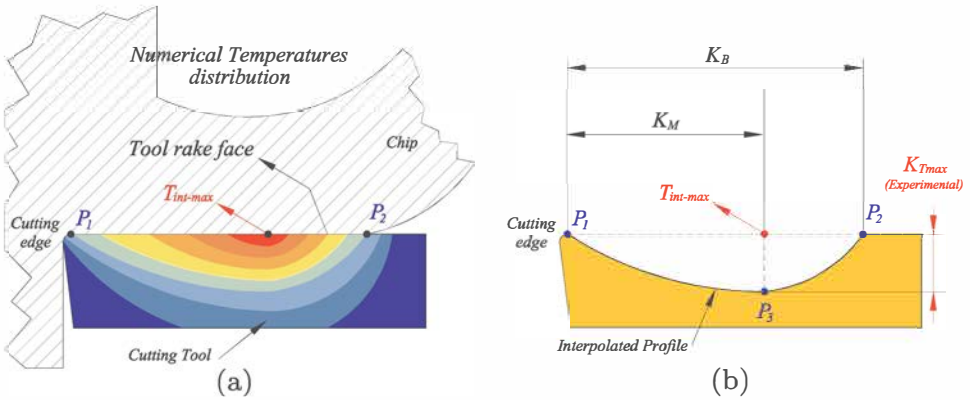

Fig. 7. Schema for interpolation of crater profiles on tool rake face: (a) numerical temperatures distribution in cutting tool, (b) interpolation of crater based on P_1, P_2 and P_3.

increasing the material hardness or strength leads to higher cutting temperatures and forces. However, machining tests show that the values of cutting forces and temperatures reached in cutting process not necessarily increases with hardness or strength of machined material. An evidence of this behaviour is the case of medium carbon steel (AISI 1045) which present higher strength and hardness compared to

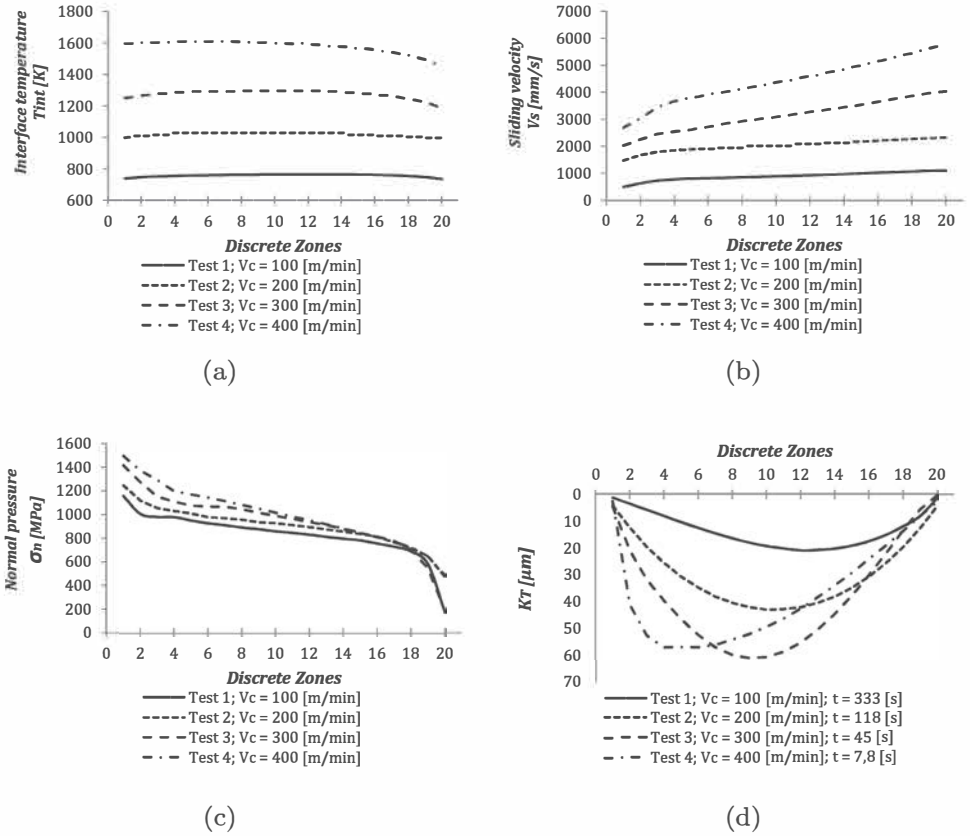

Fig. 8. Numerical wear variables distributions and Interpolated crater profiles for different cutting conditions (Table 3 – tests 1–4): (a) T_{int}, (b) V_s, (c) σ_n, (d) K_T.

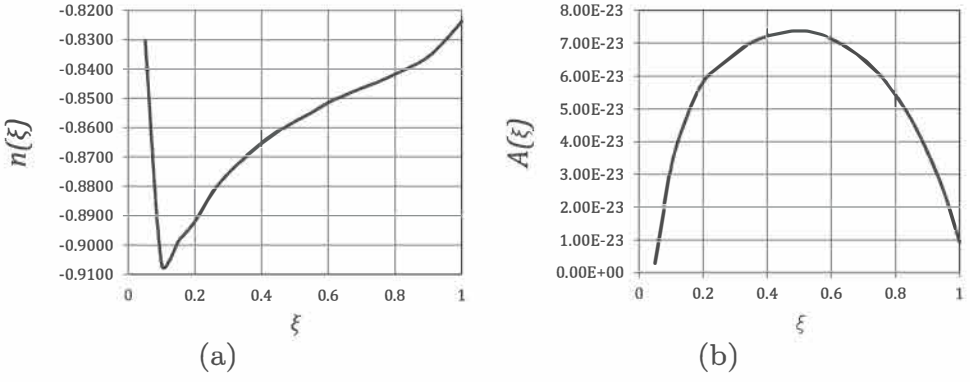

Fig. 9. A and n as functions of dimensionless position ξ along tool-chip contact.

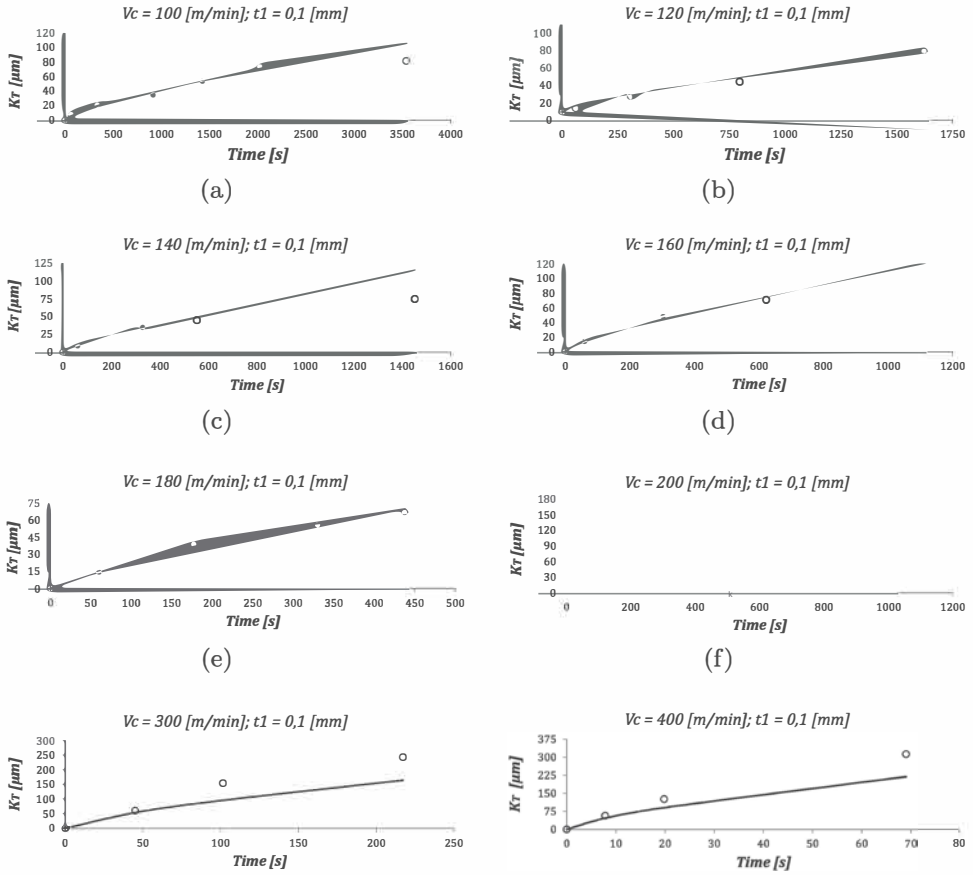

Fig. 10. Maximal depth of crater K_{Tmax} evolution: experimental data (dots) [34] and predictions made by using Eq. (15) (continuous line). Cutting conditions: AISI 1018 - WC, Cutting edge radius $R = 0.02$ [mm], feed $t_1 = 0.1$ [mm/rev], rake angle $\alpha = 0°$, Cutting speed range: $V_c = 100 - 400$ [m/min].

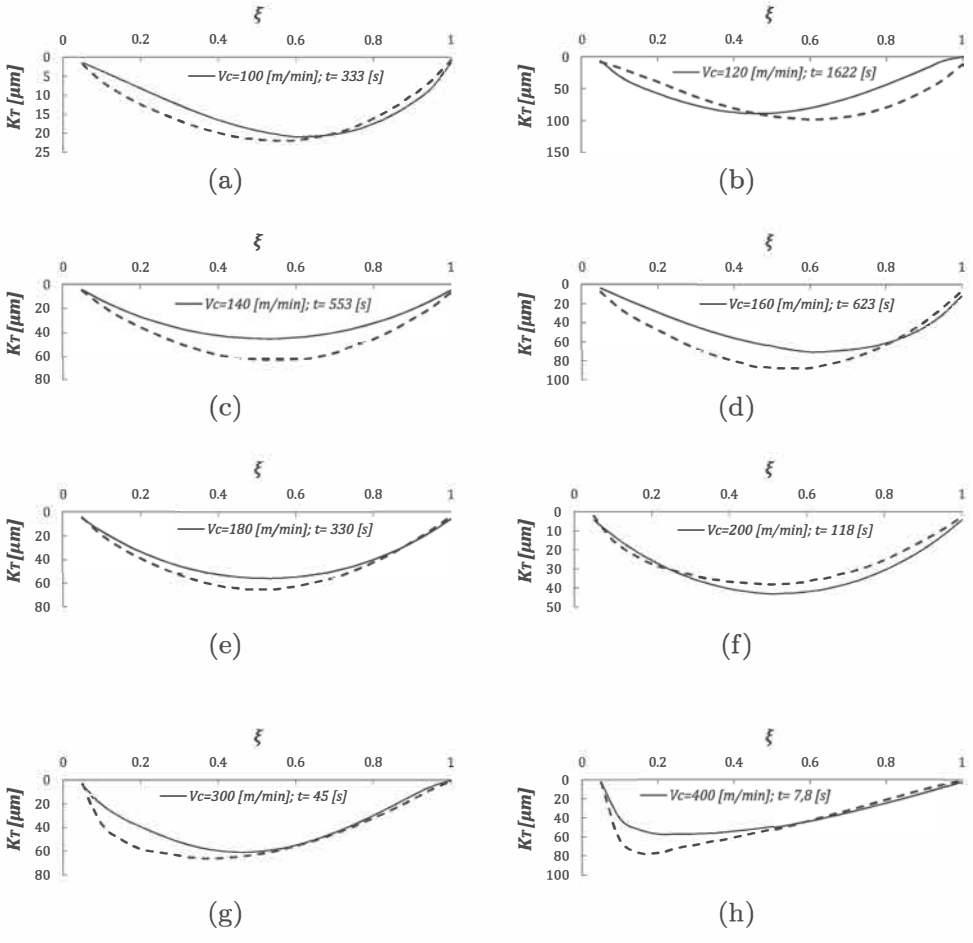

Fig. 11. Crater wear profiles at tool-chip contact: Interpolated profiles based on experimental information K_{Tmax} (continuous line) [34] y Calculated profiles by using Eq. (15) (dashed line). Cutting conditions: AISI 1018 - WC, Cutting edge radius $R = 0.02$ [mm], feed $t_1 = 0.1$ [mm/rev], rake angle $\alpha = 0°$, Cutting speed range: $V_c = 100 - 400$ [m/min].

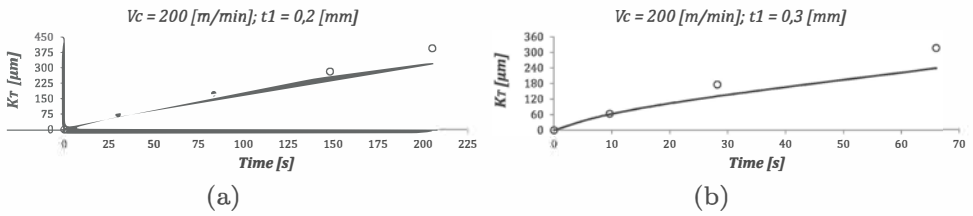

Fig. 12. Maximal depth of crater K_{Tmax} evolution: Experimental data (dots) [34] and predictions made by using Eq. (15) (continuous line). Cutting conditions: AISI 1018 - WC, Cutting edge radius $R = 0.02$ [mm], feed $t_1 = 0.2 - 0.3$ [mm/rev], rake angle $\alpha = 0°$, Cutting speed range: $V_c = 200$ [m/min].

stainless steel (AISI 316L) [65].

The above-mentioned experimental observation suggests that there is no a well defined trend about relationship between mechanical properties of work material and cutting forces and temperatures in machining. Taking account that forces (pressures) and temperatures are fundamental variables in order to estimate tool wear, the direct influence of carbon content on tool wear estimation has still to be studied in more detail. A similar discussion could be carried out for wear estimation in coated cutting tools. In that case it is important to analyze the effect of the coating over the friction and heat transfer on tool-chip interface. The methodology for wear modeling and the wear model

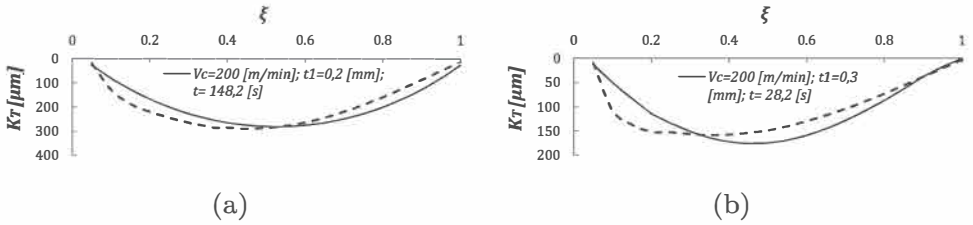

Fig. 13. Crater wear profiles at tool-chip contact: Interpolated profiles based on experimental information K_{Tmax} (continuous line) [34] y Calculated profiles by using Eq. (15) (dashed line). Cutting conditions: AISI 1018 - WC, Cutting edge radius $R = 0.02$ [mm], feed $t_1 = 0.2 - 0.3$ [mm/rev], rake angle $\alpha = 0°$, Cutting speed range: $V_c = 200$ [m/min].

developed in this work could be a good instrument in order to face the aforementioned subjects.

7. Conclusions

Tool-chip contact in steel machining with carbide cutting tool implies a complex tribological condition. A model was developed to predict evolving crater wear profiles using inputs of T_{int}, σ_n and V_s. Based on validation cutting tests on AISI 1018 steel, the model was validated and several concluding remarks can be drawn about the process of crater wear in uncoated carbide tooling material:

(a) A novel methodology based on the Vaschy-Buckingham approach has been proposed in this work for wear modeling.
(b) Based on the developed methodology plus information from numerical simulations of orthogonal cutting has been proposed a crater wear model.
(c) For steel cutting process with uncoated WC tools, the developed model was correlated and observed for a range of cutting speed from 100 to 400 m/min and feed from 0.1 to 0.3 mm.
(d) The proposed model takes into account the combined effects of the different thermo-mechanical wear mechanisms acting on the tool-chip interface. It was shown that temperature is the leading parameter followed by sliding velocity and normal pressure.
(e) For high cutting speed or high feed the model trends to underestimate crater depth. It suggests that wear rate is modified by an additional thermally activated factor which appears at high temperatures and pressures.
(f) Predictions of crater evolution and maximal crater depth location on tool rake face, made by the developed wear model, present good accordance with experimental observations.

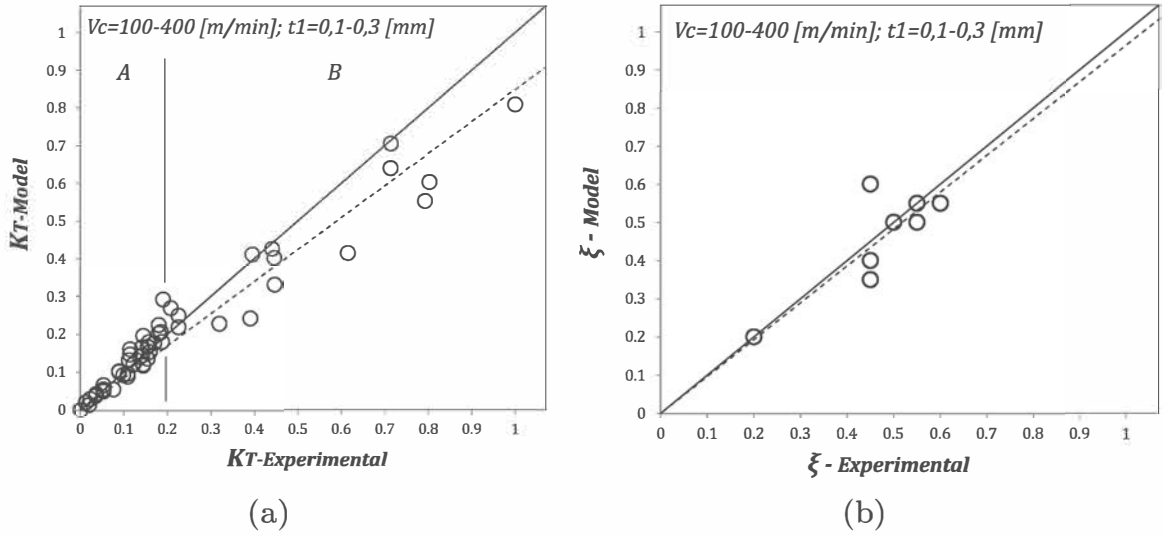

Fig. 14. Linear correlation between wear model prediction (Eq. (15)) and experimental data: (a) maximal crater depth K_T evolution. (b) Maximal crater depth location on tool rake face. Dimensionless position ξ is defined by Eq. (16).

Table 4
Approximate values of Brinell hardness, ultimate tensile strength S_{ut} and machining rate M_{rate}, for different carbon steel [65].

Carbon content	Steel	HB	S_{ut} [MPa]	M_{rate}
Base	B1112	180–220	410–510	1
Low	C1008, C1010, C1015	130–170	304–386	0.5
Medium	C1020, C1025, C1030	140–210	380–464	0.65
High	C1040, C1045, C1050	180–230	519–897	0.55

Acknowledgements

This work was supported by Secretaría Nacional de Educación Superior, Ciencia y Tecnología del Ecuador – SENESCYT, Universidad Carlos III de Madrid and the Spanish Ministry of Economy and Competitiveness and FEDER Program under Grant DPI2014-56137-C2-2-R.

References

[1] F. Klocke, G. Eisenblätter, Dry cutting, CIRP Ann. – Manuf. Technol. 46 (1997) 519–526.
[2] P. Sreejith, B. Ngoi, Dry machining: machining of the future, J. Mater. Process. Technol. 101 (2000) 287–291.
[3] P.J. Blau, Fifty years of research on the wear of metals, Tribol. Int. 30 (1997) 321–331.
[4] G. Zhao, Z. Liu, Y. He, H. Cao, Y. Guo, Energy consumption in machining: classification, prediction, and reduction strategy, Energy 133 (2017) 142–157.
[5] M. Rief, B. Karpuschewski, E. Kalhfera, Evaluation and Modeling of the Energy Demand during Machining, CIRP J. Manuf. Sci. Technol. (2017), http://dx.doi.org/10.1016/j.cirpj.2017.05.003.
[6] N. Diaz-Elsayed, D. Dornfeld, A. Horvath, A comparative analysis of the environmental impacts of machine tool manufacturing facilities, J. Clean. Prod. 95 (2015) 223–231.
[7] K. Cheng, Machining Dynamics: Fundamentals, Applications and Practices, Springer, London, 2009.
[8] M. Binder, F. Klocke, B. Doebbeler, Abrasive wear behavior under metal cutting conditions, Wear (Part A) (2017) 165–171.
[9] G. Boothroyd, W.A. Knight, Fundamentals of Machining and Machine Tools, Taylor & Francis Group, Boca Raton, FL, 2006.
[10] A. Fernández-Valdivielso, L.L. de Lacalle, G. Urbikain, A. Rodriguez, Detecting the key geometrical features and grades of carbide inserts for the turning of nickel-based alloys concerning surface integrity, Proc. Inst. Mech. Eng. Part C: J. Mech. Eng. Sci. 230 (20) (2016) 3725–3742.
[11] Iso 3685-1993: Tool Life Testing with Single Point Turning Tools.
[12] Iso 8688-1989: Tool Life Testing in Milling. Part 1: Face Milling, Part 2: End Milling.
[13] F. Taylor, On the art of cutting metals, Trans. ASME 28 (1906) 31–248.
[14] A. Molinari, M. Nouari, Modeling of tool wear by diffusion in metal cutting, Wear 252 (2002) 135–149.
[15] O. Hatt, P. Crawforth, M. Jackson, On the mechanism of tool crater wear during titanium alloy machining, Wear 374–375 (2017) 15–20.
[16] J.G. Corrêa, R.B. Schroeter, A.R. Machado, Tool life and wear mechanism analysis of carbide tools used in the machining of martensitic and supermartensitic stainless steels, Tribol. Int. 105 (2017) 102–117.
[17] R. Polvorosa, A. Suárez, L.L. de Lacalle, I. Cerrillo, A. Wretland, F. Veiga, Tool wear on nickel alloys with different coolant pressures: comparison of alloy 718 and waspaloy, J. Manuf. Process. 26 (2017) 44–56.
[18] V. Marinov, Experimental study on the abrasive wear in metal cutting, Wear 197 (1996) 242–247.
[19] R. Gohar, H. Rahnejat, Fundamentals of Tribology, Imperial College Press, London, 2008.
[20] P. Mathew, Use of predicted cutting temperatures in determining tool performance, Int. J. Mach. Tools Manuf. 29 (1989) 481–497.
[21] L. Filice, F. Micari, L. Settineri, D. Umbrello, Wear modelling in mild steel orthogonal cutting when using uncoated carbide tools, Wear 262 (2007) 545–554.
[22] J.F. Archard, Contact and rubbing of flat surfaces, J. Appl. Phys. 24 (1953) 981–988.
[23] T. Kitagawa, A. Kubo, K. Maekawa, Wear characteristics of various cutting tools in steel machining, Tribol. Ser. 32 (1997) 569–578.
[24] H. Takeyama, R. Murata, Basic investigation of tool wear, J. Eng. Ind. Trans. ASME (1963) 33–38.
[25] E. Usui, T. Shirakashi, M. Kitagawa, Analytical prediction of three dimensional cutting process, Part 3 cutting temperature and crater wear of carbide tool, Trans. Am. Soc. Mech. Eng. 100 (1978) 236–246.
[26] J.A. Olortegui-Yume, P.Y. Kwon, Local crater wear prediction using physics-based models, J. Manuf. Sci. Eng.—Trans. ASME 132 (2010) 1–9.
[27] Y. Koren, E. Lenz, Mathematical model for the flank wear while turning steel with carbide tools, Proc. CIRP Semin. Manuf. Syst. 1 (1972) 127–137.
[28] A. Malakizadi, H. Gruber, I. Sadik, L. Nyborg, An FEM-based Approach for Tool Wear Estimation in Machining, Wear 368-369 (2016) 10–24.
[29] Y.C. Yen, J. Söhner, B. Lilly, T. Altan, Estimation of tool wear in orthogonal cutting using the finite element analysis, J. Mater. Process. Technol. 146 (2004) 82–91.
[30] B. Haddag, M. Nouari, Tool wear and heat transfer analyses in dry machining based on multi-steps numerical modelling and experimental validation, Wear 302 (2013) 1158–1170.
[31] M.A. Davies, T. Ueda, R. M'Saoubi, B. Mullany, A.L. Cooke, On the measurement of temperature in material removal processes, CIRP Ann. – Manuf. Technol. 56 (2007) 581–604.
[32] A. Suárez, L.L. de Lacalle, R. Polvorosa, F. Veiga, A. Wretland, Effects of high-pressure cooling on the wear patterns on turning inserts used on alloy in 718, Mater. Manuf. Process. 32 (6) (2017) 678–686.
[33] A. Ber, S. Kaldor, The first seconds of cutting, wear behaviour, CIRP Ann. – Manuf. Technol. 31 (1982) 13–17.
[34] X. Soldani, Modélisation analytique de l'usinage à grande vitesse et étude de l'usure en cratère – Application au tournage (Ph.D. Thesis), Paul Verlaine Universite – Metz, 2008.
[35] M. Sima, T. Özel, Modified material constitutive models for serrated chip formation simulations and experimental validation in machining of titanium alloy Ti-6Al-4V, Int. J. Mach. Tools Manuf. 50 (2010) 943–960.
[36] F. Ducobu, E. Rivière-Lorphèvre, E. Filippi, On the Importance of the Choice of the Parameters of the Johnson-Cook Constitutive Model and Their Influence on the Results of a Ti6Al4V Orthogonal Cutting Model, vol. 122, 2017, pp. 143–155.
[37] A. Attanasio, E. Ceretti, A. Fiorentino, C. Cappellini, C. Giardini, Investigation and FEM-based simulation of tool wear in turning operations with uncoated carbide tools, Wear 269 (2010) 344–350.
[38] T. Özel, E. Zeren, Determination of work material flow stress and friction for fea of machining using orthogonal cutting tests, J. Mater. Process. Technol. 153–154 (2004) 1019–1025.
[39] P.J. Arrazola, T. Ozel, D. Umbrello, M. Davies, I.S. Jawahir, Recent advances in modelling of metal machining processes, CIRP Ann. – Manuf. Technol. 62 (2013) 695–718.
[40] A. Shrot, M. Bäker, Determination of Johnson–Cook parameters from machining simulations, Comput. Mater. Sci. 52 (2012) 298–304.
[41] M. Sasso, G. Newaz, D. Amodio, Material characterization at high strain rate by hopkinson bar tests and finite element optimization, Mater. Sci. Eng.: A 487 (2008) 289–300.
[42] G. List, G. Sutter, X. Bi, A. Molinari, A. Bouthiche, Strain, strain rate and velocity fields determination at very high cutting speed, J. Mater. Process. Technol. 213 (5) (2013) 693–699.
[43] N.N. Zorev, Interrelationship between shear processes occurring along tool face and on shear plane in metal cutting, Int. Res. Prod. Eng. ASME (1963) 42–49.
[44] N.N. Zorev, Metal Cutting Mechanics, Pergamos Press, Oxford, 1966.
[45] E. Lee, B. Shaffer, The theory of plasticity applied to a problem of machining, J. Appl. Mech. (1951) 15–20.
[46] X. Li, Development of a predictive model for stress distributions at the tool-chip interface in machining, J. Mater. Process. Technol. 63 (1997) 169–174.
[47] T.H.C. Childs, M.I. Mahdi, On the stress distribution between the chip and tool during metal turning, Ann. CIRP 38 (1989) 55–58.
[48] T. Childs, K. Maekawa, T. Obikawa, Y. Yamane, Metal Machining: Theory and Applications, John Wiley & Sons Inc., New York, 2000.
[49] T. Özel, The influence of friction models on finite element simulations of machining, Int. J. Mach. Tools Manuf. 46 (2006) 518–530.
[50] M. Shatla, C. Kerk, T. Altan, Process modeling in machining. Part i: determination of flow stress data, Int. J. Mach. Tools Manuf. 41 (2001) 1511–1534.
[51] P.L.B. Oxley, Mechanics of Machining: An Analytical Approach to Assessing Machinability, Ellis Horwood Limited, New York, 1989.
[52] L. Filice, F. Micari, S. Rizzuti, D. Umbrello, A critical analysis on the friction modelling in orthogonal machining, Int. J. Mach. Tools Manuf. 47 (2007) 709–714.
[53] Y.-C. Yen, A. Jain, T. Altan, A finite element analysis of orthogonal machining using different tool edge geometries, J. Mater. Process. Technol. 146 (2004) 72–81.
[54] M. Shatla, C. Kerk, T. Altan, Process modeling in machining. Part ii: validation and applications of the determined flow stress data, Int. J. Mach. Tools Manuf. 41 (2001) 1659–1680.
[55] A. Deshpande, V. Madhavan, A novel approach to accelerate attainment of thermal steady state in coupled thermomechanical analysis of machining, Int. J. Heat Mass Transf. 55 (2012) 3869–3884.
[56] F. Ramírez, Modelización de la evolución del desgaste de herramientas de corte (Ph. D. Thesis), 2015. URL: <http://hdl.handle.net/10016/22408>.
[57] K. Li, X.-L. Gao, J. Sutherland, Finite element simulation of the orthogonal metal cutting process for qualitative understanding of the effects of crater wear on the chip formation process, J. Mater. Process. Technol. 127 (2002) 309–324.
[58] G. List, G. Sutter, X.F. Bi, Investigation of tool wear in high speed machining by using a ballistic set-up, Wear 267 (2009) 1673–1679.
[59] G. List, G. Sutter, A. Bouthiche, Cutting temperature prediction in high speed machining by numerical modelling of chip formation and its dependence with crater wear, Int. J. Mach. Tools Manuf. 54–55 (2012) 1–9.
[60] T. Kitagawa, K. Maekawa, T. Shirakashi, E. USUI, Analytical prediction of flank wear of carbide tools in turning plain carbon steels (Part 1)–characteristic equation of flank wear-, Bull. Jpn. Soc. Prec. Eng. 22 (1988) 263–267.
[61] T. Kitagawa, K. Maekawa, T. Shirakashi, E. USUI, Analytical prediction of flank wear of carbide tools in turning plain carbon steels (Part 2)–prediction of flank wear-, Bull. Jpn. Soc. Prec. Eng. 23 (Part 2) (1989) 126–134.
[62] L.-J. Xie, J. Schmidt, C. Schmidt, F. Biesinger, 2D FEM estimate of tool wear in turning operation, Wear 258 (2005) 1479–1490.
[63] W. Grzesik, Advanced Machining Processes of Metallic Materials: Theory, Modelling and Applications, Elsevier Science, Amsterdam, Boston, 2008.
[64] L.N.L. de Lacalle Maracaide, J.A.S. Galíndez, A.L. Menchaca, Mecanizado de Alto Rendimiento: Procesos de Arranque, EDICIONES TÉCNICAS IZARO, 2004.
[65] M.P. Groover, Fundamentals of Modern Manufacturing: Materials, Processes, and Systems, John Wiley & Sons, 2010.